NANO LETTERS

2006
Vol. 6, No. 11
2531−2535

Experimental Observation of Nonlinear Ionic Transport at the Nanometer Scale

Diego Krapf, Bernadette M. Quinn, Meng-Yue Wu, Henny W. Zandbergen, Cees Dekker, and Serge G. Lemay*

Kavli Institute of Nanoscience, Delft University of Technology, Lorentzweg 1, 2628 CJ Delft, The Netherlands

Received August 18, 2006; Revised Manuscript Received September 25, 2006

ABSTRACT

Nanometer-sized electrodes are used to probe the transport of ions in liquid by monitoring heterogeneous electrochemical reactions. We observe pronounced nonlinearities of ion flux versus concentration when transport is localized within a region smaller than 10 nm. We show that these observations cannot be explained using conventional continuum, mean-field descriptions of ionic transport. The data indicate that these deviations are caused by the high flux of charged species that is achieved at nanometer-sized electrodes.

Understanding ionic transport in liquid near charged interfaces is an outstanding theoretical and experimental challenge of particular relevance to the emerging field of nanofluidics. The equilibrium distributions and transport properties of ionic systems are most commonly described using the Poisson−Boltzmann (PB) and Poisson−Nernst−Planck (PNP) formalisms, respectively. Such continuum, mean-field descriptions can break down on sufficiently small length scales because they take into account neither the discreteness and finite size of the mobile ions nor the structure of the solvent. Experiments that probe these microscopic length scales directly are now becoming possible. For example, recent X-ray scattering measurements of the equilibrium ion distribution near charged interfaces[1,2] and DNA molecules[3] required taking into account the effect of local chemical equilibrium,[1] finite ion sizes,[3] or molecular-scale solvent structure.[2]

Compared to equilibrium properties, the transport of ions near charged interfaces remains poorly understood. The difficulty lies in disentangling the contributions from electrostatics, hydrodynamics, and solvent structure on the scale of a few nanometers. Several recent experimental studies have concentrated on ionic transport parallel to charged interfaces, which can be probed in systems ranging from colloids[4] to synthetic[5,6] or biological[7,8] nanochannels. Transport perpendicular to an interface, however, couples more directly to the electrostatic potential induced by surface charges. A powerful method for measuring conductance across the double layer is electrochemistry, where charge transfer between redox molecules in solution and an electrode provides a probe of ionic transport. Although the Nernst−Planck equation with the electroneutrality approximation was initially applied to this problem,[9,10] the advent of nanometer-scale electrodes[11] revived the question of the validity of this simple approach.[12,13] More recently, anomalous transport to submicrometer electrodes was observed upon removal of supporting electrolyte,[14−16] which was attributed to the interfacial electric field.

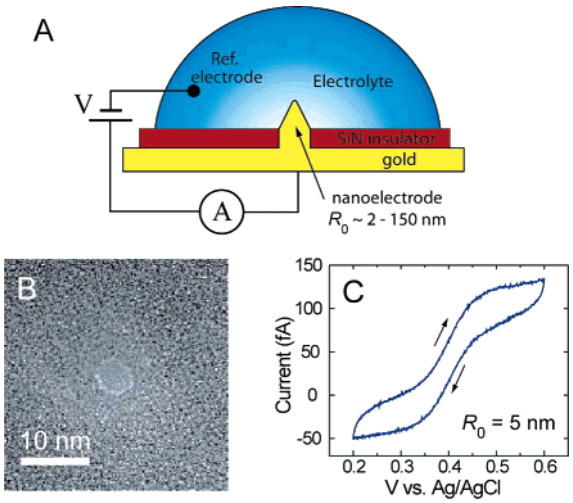

Figure 1. (A) Schematic representation of the experimental setup. A nanoelectrode is immersed in solution, a potential is applied, and the current is recorded. (B) Transmission electron microscopy image of a pore with radius 2.5 nm in a SiN membrane. (C) Voltammetric response of an electrode 5 nm in radius (0.1 mM $FcTMA^+$ in 0.5 M NH_4NO_3).

Here we study ion transport using gold electrodes with radii of only a few nanometers. This size approaches both the typical interionic spacing and the Debye screening length, even in high ionic strength solutions. As illustrated in Figure 1A, a nanoelectrode is immersed in an electrolyte and biased

* Corresponding author. Fax: +31-15-2781202; e-mail: lemay@mb.tn.tudelft.nl.

10.1021/nl0619453 CCC: $33.50
Published on Web 10/07/2006

so as to drive an electron-transfer reaction with an ionic species in solution. The electrical current through the electrode provides a direct measure of the flux of ions transported to the electrode surface. Because the concentration gradient is localized within a length scale comparable to the dimensions of the nanoelectrode, extremely steep stationary concentration gradients are achieved and transport properties are probed on the scale of several nanometers. As a result of this abrupt concentration gradient, exceptionally high ionic fluxes are reached. We find that the classical mean-field approximation does not describe ionic transport adequately in this regime. Specifically, the data indicate that the PNP formalism fails because of the nonequilibrium conditions induced at the electrical double layer.

To carry out these experiments, we developed a method for fabricating nanoelectrodes with a well-defined geometry and independently determined dimensions. The latter is particularly important to the present work: in previous studies, an effective radius was typically deduced from the steady-state electrochemical current itself without the possibility of independently characterizing electrodes smaller than ~50 nm.[11−16] We show below that the current no longer scales linearly with electrode size for radii below ~10 nm, invalidating this procedure.

The details of the electrode fabrication process were reported previously.[17] In brief, we first fabricated a 20-nm-thick free-standing SiN membrane using standard microfabrication technology. Pores with radii between 2 and 150 nm were then drilled in the thin membranes with a focused electron beam.[18,19] Following pore formation, high-resolution transmission electron microscopy was used to determine the radius of each individual pore with subnanometer accuracy (Figure 1B). The pores were subsequently filled with gold to yield convex electrodes with a diameter equal to that of the pore, as sketched in Figure 1A.

Ferrocenylmethyltrimethylammonium ($FcTMA^+$) and ferrocenedimethanol ($Fc(CH_2OH)_2$) were employed as electroactive species. $FcTMA^+$ is oxidized at the electrode surface to become $FcTMA^{++}$ at a formal potential of 0.42 V with respect to a Ag/AgCl reference. $Fc(CH_2OH)_2$ is neutral and is oxidized to $Fc(CH_2OH)_2^+$ at 0.25 V. For the electrochemical measurements, a standard 3 M Ag/AgCl electrode served as both reference- and counter-electrode. The oxidation of the redox species was recorded using home-built electronics. Our preamplifier had a 3 Hz bandwidth and 2 fA rms noise. Each data point was integrated over a period of 1 s following a 1 s delay, ensuring that we measured the steady-state current. Ion concentrations were deduced from the diffusion-limited current at a commercial 10 μm disc electrode.[20]

Excess electroinactive NH_4NO_3 (0.5 M) was added to the solutions as base electrolyte (Debye length ≈ 0.4 nm). Electrochemical currents are governed by both the transport of reactants to the electrode and the electron-transfer rate at the solution−electrode interface. The latter varies exponentially with the electrode potential.[21] Because we are interested in probing ionic transport, we concentrate on potentials where charge-transfer kinetics do not play any role. This situation is always achieved at sufficiently high potentials, where

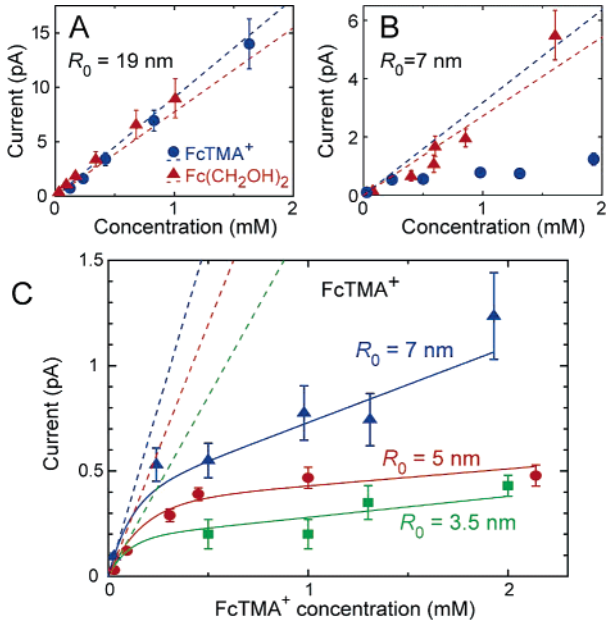

Figure 2. (A) Transport-limited current as a function of $FcTMA^+$ concentration and $Fc(CH_2HO)_2$ at an electrode 19 nm in radius and (B) at an electrode 7 nm in radius. The dashed lines show the expected behavior (no fitting parameters). (C) Transport-limited current as a function of concentration of $FcTMA^+$ in electrodes with radii of 3.5, 5, and 7 nm. Solid lines are guides to the eye, and dashed lines show the expected diffusion-driven current based on the known electrode size.

electron-transfer is extremely fast (i.e., $V - V_0 \gg KT/e$, where V is the applied potential and V_0 is the formal potential of the reaction).

A typical cyclic voltammogram (current−voltage response) is shown in Figure 1C. The current reaches a plateau, indicating that it is independent of heterogeneous kinetics and is controlled by ionic transport at potentials higher than 0.5 V. In addition to the faradaic current, a finite slope and a hysteretic offset are observed between the forward and backward scans because of the parasitic dielectric response of the insulating membrane.[17] Two methods were used to subtract these dielectric currents: either voltammograms of solutions containing no electroactive ions were recorded and subtracted from the original data or the electrode was set at the plateau potential and the current was measured until stable. Both methods yielded the same results.

Transport-limited currents (plateaus in the voltammograms) at an electrode 19 nm in radius for different ionic concentrations are shown in Figure 2A. The currents, and therefore the ionic fluxes, vary linearly with concentration. This is consistent with the widely used assumption that in the presence of excess supporting electrolyte, mass-transport is dominated by diffusion of the redox species.[10,21] At a hemispherical electrode, this yields $i_D = 2\pi enDR_0$, with n being the ion number density, D being the diffusion coefficient, and R_0 being the electrode radius. The dashed lines in the figure show the predicted behavior approximating the geometry of our electrodes to a hemisphere using the measured radius and known diffusion constants. These curves match the data quite well without any adjustable parameters.

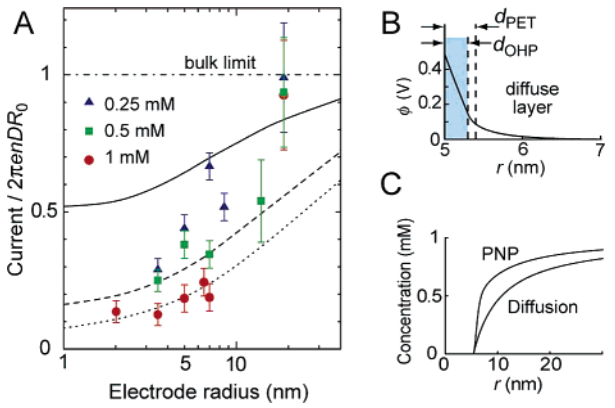

Figure 3. (A) Transport-limited current of $FcTMA^+$ normalized to the calculated diffusion-limited current as a function of electrode radius for eight electrodes and three different ion concentrations: 0.25, 0.5, and 1 mM. The lines are solutions of the PNP equations with $d_{OHP} = 0.3$, 0.3, and 0.18 nm and $d_{PET} = 0.4$, 0.3, and 0.18 nm (solid, dashed, and dotted lines respectively). (B) Potential at a 5 nm electrode calculated using PNP. The outer Helmholtz plane (1.3 nm) and the plane of electron-transfer (1.4 nm) are shown. (C) Simulation results showing a comparison bewteen $FcTMA^+$ concentration obtained using PNP and pure diffusion.

Strong deviations from the simple diffusive behavior are observed for electrodes with sub-10-nm dimensions. As shown in Figure 2C, transport to these electrodes is no longer linear with $FcTMA^+$ concentration, instead increasing in a sublinear manner. The predicted diffusion-driven currents are also shown in the Figure, showing that the current is suppressed when the $FcTMA^+$ concentration exceeds ~0.2 mM. This dramatic departure from classical diffusion occurs for the charged $FcTMA^+$ but was not observed for electroneutral $Fc(CH_2OH)_2$, as shown in Figure 2B. This behavior indicates that the current suppression is induced by coupling of the charged species to the electric field.

Figure 3A shows the limiting currents at 8 electrodes with radii in the 2−20 nm range using different $FcTMA^+$ concentrations. The electrode potential and base electrolyte concentration for all data presented here were 0.5 V and 0.5 M, respectively. To compare electrodes of different sizes, the measured currents were normalized to the calculated diffusion-driven current, i_D, based on the known electrode radius. The measured currents are systematically smaller than the expected diffusion-driven values ($i/i_D < 1$), and the degree of suppression is greater the higher the $FcTMA^+$ concentration and the smaller the electrode size.

The failure of pure diffusion to account for our observations with charged redox molecules is expected because the size of our electrodes starts to approach the values of both the Debye length and the size of the ions. The interfacial electric field should therefore affect the transport of charged molecules. Nonetheless, because the base electrolyte concentration was kept constant and much greater than the $FcTMA^+$ concentration, the electric field is expected to be independent of electroactive species concentration. A strong nonlinear dependence on electroactive ion concentration, such as that seen in Figure 2C, is therefore extremely surprising.

We now demonstrate that this effect cannot be captured by the PNP formalism, which has been used (in either full or simplified forms) to describe practically all electron transfer measurements at nanoelectrodes to date.[9−16,22] In the absence of convective flows, the PNP equations are

$$\epsilon\nabla^2\phi = -e\Sigma z_i n_i \quad (1)$$

$$\vec{J}_i = -D_i\left(\vec{\nabla}n_i + \frac{z_i e}{kT} n_i \vec{\nabla}\phi\right) \quad (2)$$

where ϕ is the electrostatic potential, ϵ is the electric permittivity, $\vec{J}_i$ and z_i are the flux and valence of ion species i, respectively, and the rest of the symbols were defined above. Subindex i spans the four species involved in the problem: two for the base electrolyte ($z = \pm 1$) and two for the electroactive molecules ($z = +1$; $+2$ for FcTMA). In steady state, mass conservation implies $\vec{\nabla}\cdot J_i = 0$ for the redox couple and $\vec{J}_i = 0$ for the inert ions. We employ standard boundary conditions for the electrode surface. Namely, the electrode is treated in terms of an outer Helmholtz plane (OHP) and a plane of electron transfer (PET, Figure 3B). The OHP serves as the plane of closest approach of ions to the electrode surface. The region between the electrode surface proper and the OHP has zero charge density, and continuity is maintained for ϕ and $\vec{\nabla}\phi$ at the OHP. We allow electron transfer to occur further away than the OHP, at a distance d_{PET} from the surface. At the PET, the reactant concentration is zero (fast electron-transfer approximation) and the product flux equals the reactant flux with opposite sign (mass conservation).

The equations were solved numerically using a finite elements package (Comsol Multiphysics). We considered a hemispherical electrode geometry so that the problem simplified to spherical symmetry. The resulting potential and $FcTMA^+$ concentration profiles for a 5 nm electrode are plotted in Figure 3B and 3C. The electrode potential is not uniquely defined because the potential of zero charge (pzc) of the system is not known. However, the pzc of gold versus Ag/AgCl is on the order of 0.04 V.[15] We checked that the simulations are not sensitive to changes in the electrode voltage within the relevant range of 0.4−0.6 V and that our results are not qualitatively changed by this potential. Although the distances d_{OHP} and d_{PET} can be estimated, their exact values cannot be calculated and are generally determined empirically. We therefore performed calculations over a broad range of parameters. Typical results are represented in Figure 3A. Suppression of the current is indeed predicted with decreasing electrode size below 50 nm, which has its physical origin in the overlap between the diffusion region and the electrical double layer.[13−15,22] Results are essentially insensitive to the position of the OHP (for physically relevant values of 0.2−0.4 nm). The current is, however, very sensitive to d_{PET}. In particular, the degree of suppression increases with decreasing d_{PET}, consistent with the rapid decay of the (equilibrium) electrostatic potential with distance from the electrode.

Most relevant to our experimental observations, PNP predicts that the normalized current, i/i_D, is insensitive

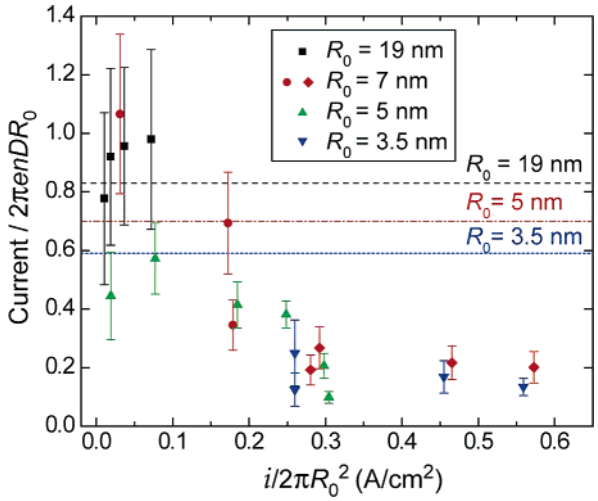

Figure 4. Normalized transport-limited current as a function of current density for electrodes with radius between 3.5 and 19 nm. The three lines show the PNP solutions with OHP at 0.3 nm and charge transfer at 0.4 nm for electrode radii of 19, 5, and 3.5 nm.

(difference invisible on the scale of Figure 3A) to the concentration of electroactive ions within the range of concentrations probed, contradicting the data in Figures 2C and 3A. Although Figure 3A shows that individual data sets at particular concentrations can be fitted adequately by selecting appropriate values for d_{PET}, the parameters obtained are not physical. Data at different concentrations require different values of d_{PET} and are impossible to fit with a single choice of this parameter. Because d_{OHP} and d_{PET} represent local interactions between individual ions and the electrode, they cannot depend on the electroactive ion concentration. We conclude that the conventional PNP model fails to explain the pronounced nonlinearity of the electrochemical current with concentration.

Suppression of the current is observed for electrode radii comparable to or smaller than the average spacing between electroactive ions, $R_0 \approx n^{-1/3} \approx 10-20$ nm. Figures 2C and 3A, however, show that for a given electrode size the degree of suppression increases with increasing ion concentration. This indicates that this crossover in length scales is not responsible for the current suppression.

Some understanding of this surprising effect is gained by focusing on the nonequilibrium conditions at the electrode surface. Figure 4 shows the observed degree of suppression, i/i_D, versus the measured current density at the electrode $i/2\pi R_0^2$. The latter is a measure of how far the system is driven from equilibrium. Data for different electrodes collapse within error unto a single curve. At low current densities, i/i_D approaches unity and pure diffusion provides an adequate estimate of the measured current. At current densities less than ~0.15 A/cm^2, the current is suppressed below the expected value for pure diffusion but still lies within experimental error of the values expected from the PNP calculations. At current densities above ~0.15 A/cm^2, significant additional suppression is observed, which cannot be described by PNP.

This analysis implies that the simple PNP model breaks down in the vicinity of the electrode when the system is driven sufficiently far from equilibrium. Deviations are thus observed at nanoelectrodes because much higher flux densities can be achieved rather than because of a crossover in length scales. Therefore, the observed critical radius is set by the electrode size at which sufficiently high current densities are attained for practical ionic concentrations (i.e., within the solubility limit). Limits to the validity of the mean-field approximation are relatively well-understood for equilibrium distributions of ions, but this is not true for dynamical situations, especially for high current densities within small length scales that were previously experimentally inaccessible. Recently, several authors have questioned the applicability of transport continuum models to nanoscale systems.[23−25] Ion permeation through biological channels was simulated using all-atom molecular dynamics (MD)[26,27] as well as Brownian dynamics.[23,24] It was concluded that the PNP formalism does not capture the physics of small volumes involving the statistics of few ions. This analysis has not yet been brought to bear on electrochemical problems, however. Here, additional mechanisms neglected in PNP are likely to become significant far from equilibrium, including hydrodynamic coupling, which appears to not play an important role in ionic channels. Furthermore, the diffusive transport of individual ions is coupled via collective effects such as counterion atmosphere relaxation and associated density fluctuations, which can be described using, for example, mode coupling theory.[28] Disentangling these effects will, however, require extensive theoretical work.

In summary, we have performed reliable measurement of ionic transport at independently characterized nanoelectrodes. We observed a pronounced deviation from predictions based on continuum models for electrodes smaller than ~10 nm. This behavior is governed by the ion flux at the electrode surface. This demonstrates the need for more advanced models to describe far-from-equilibrium ionic transport when high ion fluxes are attained locally in nanometer domains.

Acknowledgment. This work was funded by NanoNed, FOM, and NWO.

References

(1) Bu, W.; Vaknin, D.; Travesset, A. *Phys. Rev. E* **2005**, *72*, 060501-(R).
(2) Luo, G.; Malkova, S.; Yoon, J.; Schultz, D. G.; Lin, B.; Meron, M.; Benjamin, I.; Vanysek, P.; Schlossman, M. L. *Science* **2006**, *311*, 216.
(3) Andresen, K.; Das, R.; Park, H. Y.; Kwok, L. W.; Lamb, J. S.; Smith, H.; Herschlag, D.; Finkelstein, K. D.; Pollack, L. *Phys. Rev. Lett.* **2004**, *93*, 248103.
(4) Lyklema, J. *J. Phys.: Condens. Matter* **2001**, *13*, 5027.
(5) Ho, C.; Qiao, R.; Heng, J. B.; Chatterjee, A.; Timp, R. J.; Aluru, N. R.; Timp, G. *Proc. Natl. Acad. Sci. U.S.A.* **2005**, *102*, 10445.
(6) Siwy, Z.; Kosinska, I. D.; Fulinski, A.; Martin, C. R. *Phys. Rev. Lett.* **2005**, *94*, 048102.
(7) Läuger, P. *Biochim. Biophys. Acta* **1976**, *455*, 493.
(8) Bezrukov, S. M.; Kasianowicz, J. J. *Phys. Rev. Lett.* **1993**, *70*, 2352.
(9) Amatore, C.; Fosset, B.; Bartelt, J.; Deakin, M. R.;Wightman, R. M. *J. Electroanal. Chem.* **1988**, *256*, 255.
(10) Myland, J. C.; Oldham, K. B. *J. Electroanal. Chem.* **1993**, *347*, 49.
(11) Penner, R. M.; Heben, M. J.; Longin, T. L.; Lewis, N. S. *Science* **1990**, *250*, 1118.

(12) Oldham, K. B.; Bond, A. M. *J. Electroanal. Chem.* **2001**, *508*, 28.
(13) Smith, C. P.; White, H. S. *Anal. Chem.* **1993**, *65*, 3343.
(14) Chen, S.; Kucernak, A. *J. Phys. Chem. B* **2002**, *106*, 9396.
(15) Watkins, J. J.; White, H. S. *Langmuir* **2004**, *20*, 5474.
(16) Conyers, J. L.; White, H. S. *Anal. Chem.* **2000**, *72*, 4441.
(17) Krapf, D.; Wu, M. Y.; Smeets, R. M. M.; Zandbergen, H. W.; Dekker, C.; Lemay, S. G. *Nano Lett.* **2006**, *6*, 105.
(18) Storm, A. J.; Chen, J. H.; Ling, X. S.; Zandbergen, H. W.; Dekker, C. *Nat. Mater.* **2003**, *2*, 537.
(19) Wu, M. Y.; Krapf, D.; Zandbergen, M.; Zandbergen, H.; Batson, P. E. *Appl. Phys. Lett.* **2005**, *87*, 113106.
(20) Diffusion coefficients were taken as 0.75×10^{-5} cm^2/s for $FcTMA^{+}$ [16] and 0.64×10^{-5} cm^2/s for $Fc(CH_2OH)_2$. Zhang, W.; Gaberman, I.; Ciszkowska, M. *Electroanalysis* **2003**, *15*, 409.
(21) Bard, A. J.; Faulkner, L. R. *Electrochemical Methods: Fundamentals and Applications*, 2nd ed.; Wiley: New York, 2001.
(22) He, R.; Chen, S. L.; Yang, F.; Wu, B. L. *J. Phys. Chem. B* **2006**, *110*, 3262.
(23) Corry, B.; Kuyucak, S.; Chung, S. H. *Biophys. J.* **2000**, *78*, 2364.
(24) Yu, S.; Im, W.; Roux, B. *Biophys. J.* **2004**, *87*, 2299.
(25) Schuss, Z.; Nadler, B.; Eisenberg, R. S. *Phys. Rev. E* **2001**, *64*, 036116.
(26) Roux, B.; Allen, T.; Bernèche, S.; Im, W. *Q. Rev. Biophys.* **2004**, *37*, 15.
(27) Aksimentiev, A.; Schulten, K. *Biophys. J.* **2005**, *88*, 3745.
(28) Chandra, A.; Bagchi, B. *J. Phys. Chem. B* **2000**, *104*, 9067.

NL0619453